JPE 13-5-4

http://dx.doi.org/10.6113/JPE.2013.13.5.766

# Single-Ended High-Efficiency Step-up Converter Using the Isolated Switched-Capacitor Cell

Do-Hyun Kim*, Jong-Ho Jang*, Joung-Hu Park†**, and Jung-Won Kim**

*†Dept. of Electrical Engineering, Soongsil University, Seoul, Korea.
**Silicon Mitus, Inc., Seoul, Korea

**Abstract**

The depletion of natural resources and renewable energy sources, such as photovoltaic (PV) energy, has been highlighted for global energy solution. The PV power control unit in the PV power-generation technology requires a high step-up DC–DC converter. The conventional step-up DC–DC converter has low efficiency and limited step-up ratio. To overcome these problems, a novel high step-up DC–DC converter using an isolated switched capacitor cell is proposed. The step-up converter uses the proposed transformer and employs the switched-capacitor cell to enable integration with the boost inductor. The output of the boost converter and isolated switched-capacitor cell are connected in series to obtain high step-up with low turn-on ratio. A hardware prototype with 30 V to 40 V input voltage and 340 V output voltage is implemented to verify the performance of the proposed converter. As an extended version, another novel high step-up isolated switched-capacitor single-ended DC–DC converter integrated with a tapped-inductor (TI) boost converter is proposed. The TI boost converter and isolated-switched-capacitor outputs are connected in series to achieve high step-up. All magnetic components are integrated in a single magnetic core to lower costs. A prototype hardware with 20 V to 40 V input voltage, 340 V output voltage, and 100 W output power is implemented to verify the performance of the proposed converter.

**Key words:** Boost converter, Isolated switched-capacitor cell, Single-ended, Tapped-inductor

## I. INTRODUCTION

Low-voltage high-current renewable energy sources require high voltage step-up to be integrated in commercial power lines. The photovoltaic (PV) power generation technology, which attracts great attention as a next-generation energy source, essentially requires a high step-up DC–DC converter [1]-[5]. The boost converter tends to restrict the boosting ratio for applications with large gap between input and output voltage because these applications require extremely high duty cycle of the main switch for high step-up voltage [6]–[8]. This operation leads to the stress increase of voltage or of current on the switches and diodes, as well as the increase in diode-switching loss caused by reverse recovery characteristics. Conversion efficiency is eventually decreased by increasing the main switch loss, diode loss, and electromagnetic interference noise. Thus, additional circuits, such as coupled inductors or voltage multipliers, are necessary for the boost converter for applications in high step-up conditions [9]–[24]. The coupled-inductor method is a voltage-enhancement technique that uses core-sharing magnetic devices that integrate the functions of auto-transformers and inductors. This method is generally suitable to high-current applications. The voltage multiplier method is another enhancement technique that uses high-voltage capacitors and diodes [4], [11]–[14], [22], [23]. This method has a simple hardware; however, the output voltage of this method has discrete levels because of the absence of voltage regulation capability. We can realize an extreme voltage-gain power conversion circuit by applying both techniques.

Some previous attempts at applying these engineering techniques to high step-up converter topologies, particularly for low-voltage power sources, have reported some limitations. A previous article [10] mentioned that in a clamp-mode couple-inductor buck–boost converter [16], the output diode stress was similar to that of a traditional flyback converter, i.e., the output diode stress was higher than the output voltage even though the leakage energy from the

Manuscript received Mar. 2, 2013; revised Jul. 1, 2013
Recommended for publication by Associate Editor Yan Xing.
†Corresponding Author: wait4u@ssu.ac.kr
Tel: +82-2-828-7269, Fax: +82-2-817-7961, Soongsil University
*Dept. of Electrical Engineering, Soongsil University, Korea
**Silicon Mitus, Inc., Korea

coupled-inductor was recycled to reduce system losses. Another drawback of the converter was the high input current ripple that existed because no current path was present when the metal–oxide–semiconductor field-effect transistor (MOSFET) was off. Further improvements of the step-up converter were accomplished by combining a boost converter with a flyback converter [17], [18]. Compared with the converter in [16], the boost ratio was improved as a result of the outputs of the boost converter and flyback converter in series. Nevertheless, the same problem in [16] remained. By adding a switched-capacitor in series with the transformer, a new high boost ratio DC–DC converter with coupled-inductor and switched capacitor was introduced [19]. With the switched-capacitor between the primary side and the secondary side of the coupled-inductor, the boost ratio increased and the output diode voltage stress was reduced. However, the magnetic core is not fully utilized because the operation includes only an inductor mode and not a transformer mode. An improved version is presented in [10]. This version combines pulse-width modulation and resonant power conversions to increase the total power delivered and to decrease losses through simultaneous energy transfer in an auxiliary inductor and a charge-pump capacitor. However, this version needs more components for energy transfer. The design complexity also needs to be enhanced, and the material cost needs to be lowered.

This paper proposes a novel converter that couples a new switch-capacitor cell to the inductor of the boost converter through a high step-up isolation transformer. This approach is made to enable high step-up with low turn-on ratio by using the series connection of the output. The magnetically integrating idea of switched capacitors and boost converters, in which each of the magnetic energy transfer modes is combined in an alternatively delivering manner, is introduced in the proposed high boost ratio DC–DC converter. The continuous energy transfer during the switch-on and switch-off in every switching cycle can increase the total power delivery and can decrease the losses in the circuit. In this approach, energy is transferred through a single-core integrated transformer, which combines the modes and operates as an energy storage. As a result, the magnetic core can be used more effectively, and smaller magnetics can be employed [1], [10]. The continuous input current of the converter causes smaller current ripple than that of previous high boost ratio converter topologies employing coupled-inductors. A lower input current ripple is useful in decreasing input capacitance and in implementing maximum power point tracking for PV modules. The conduction losses in the primary side of the transformer are greatly reduced because of the reduced input current root mean square (RMS) through the primary side. Furthermore, the proposed method significantly decreases the voltage rating of the main switch or the diodes on the boost converter by properly adjusting the turn ratio of the transformer as well as by expanding the design criteria for component selection. The single-ended circuit system of the new converter is relatively simple and cost-effective. The converter is also extremely efficient with low turn-on ratio.

As an extended topology from the isolated switched-capacitor boost converter, another novel converter that uses a tapped-inductor (TI) and an isolated voltage multiplier is proposed. The topology has a step-up voltage with low turn-on ratio by using the series connection of each output [9]. The proposed method decreases the voltage rating of the diodes and the turn-on ratio of the main switch in the non-isolated TI boost converter by appropriately adjusting both turns ratios of the transformer in the cell and of the TI. This adjustment leads to a one-step further extension of the design criteria for device component selection. The circuit configuration of the proposed converter is single-ended and is highly efficient in a wide input range.

The remainder of this study is organized as follows. Section II proposes a new isolated switched-capacitor cell with coaxial cable transformer. Section III presents the operating analysis of the proposed series-output isolated switched-capacitor boost converter scheme. In Section IV, the experimental results of a 150W hardware prototype as a pre-regulating stage of the multi-stage PV power conditioning system are given for topology verification. Section V presents the operating analysis of a new version of the extended step-up converter that employs a TI. Section VI presents the experimental results of a 100W hardware prototype. Lastly, the conclusion is discussed in Section VII.

## II. ISOLATED SWITCHED-CAPACITOR CELL

### *A. Isolated Switched-Capacitor Cell*

Switched-capacitor or charge-pump circuits are generally applied for step-up converters [11]-[14]. However, the circuits have a limitation in terms of augmenting the output voltage. Multiple-stage structures should be used in spite of the power efficiency reduction. Aside from power loss, poor output voltage regulation with discrete voltage gain is also a drawback of step-up converters. To cope with these problems, we introduce a new switched-capacitor circuit that includes a transformer. The proposed circuit has isolation capability and high step-up ratio through the use of a high turn-ratio transformer. Given that the transformer is ideal, the operating principle is quite similar to that of conventional switched capacitors. In this paper, we named the proposed cell *isolated switched-capacitor cell.* However, the secondary winding coil of the transformer has parasitic resistance, which results in various operating waveforms of the circuit.

The structure of the proposed switched-capacitor cell is shown in Fig. 1. Regardless of the switching frequency or

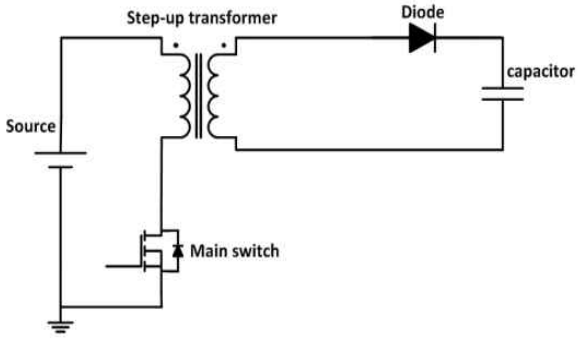


Fig. 1. Isolated switched-capacitor cell

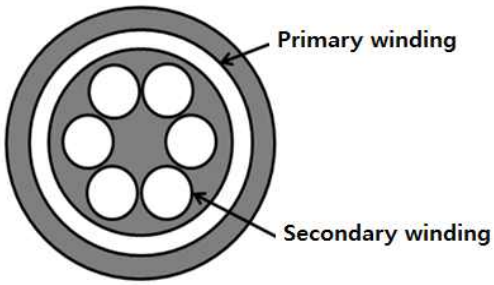


Fig. 2. Cross-section of a coaxial cable

duty ratio, the turns ratio of the winding of a transformer determines the boost operation of a cell. The turns ratio can be described as follows:

$$V_{c\_cp} = \frac{N_s}{N_p} V_p \quad . \quad (1)$$

The step-up ratio is independent of the magnetizing inductance of the transformer.

A transformer generally involves leakage inductance because of its imperfect coupling. If leakage inductance is contained in the isolated charge pump cell, the waveform of the current flowing on the secondary diode turns into LC resonance. When the size of leakage inductance is negligible, the peak point of the resonance curve occurs at every switching turn-on time. The growth of the leakage inductance moves the peak point far away from the turn-on time, i.e., the peak point of the diode current of the charge pump cell changes because of the leakage inductance size. Leakage inductance also decreases the power efficiency of the transformer. Considering that a good coupling transformer is necessary to make highly efficient cells, we use a coaxial cable transformer.

Coaxial cable winding is considered better than sandwich winding in terms of magnetic flux-linkage [25]. The coaxial cable transformer is made of high-voltage side coils and low-voltage side-winding coil that cover the high-voltage coils. Fig. 2 provides a cross-section of a coaxial cable. The coaxial cable transformer has a coupling constant of 0.9999418.

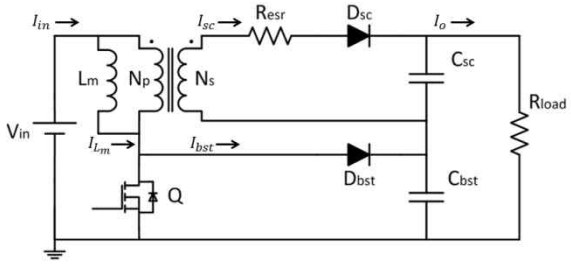


Fig. 3. Circuit diagram of the proposed converter.

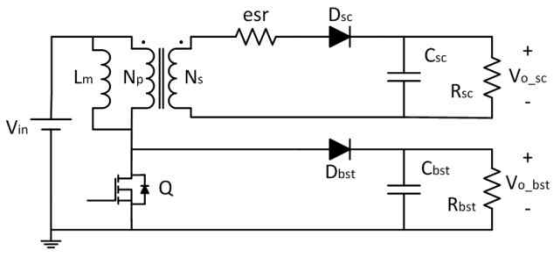


Fig. 4. Equivalent circuit of the proposed converter with separated outputs.

### *A. Reset Circuit*

In a normal operation of isolated charge pump, a reset circuit is required to reset the magnetizing current similar to that of typical forward converters. The output of the reset is tied to the switched-capacitor output. Therefore, the reset works as a boost converter to the entire load (see Fig. 3). The poor output regulation of the switched-capacitor can be relieved by the contribution of the boost regulation. Therefore, the series-connected reset circuit is recommended not only for the step-up but also for the control of the step-up output voltage in a DC–DC converter of the PV power generation system.

## III. SERIES-CONNECTED ISOLATED SWITCHED-CAPACITOR BOOST CONVERTER

### *A. Structure of the Proposed Converter*

The structure of the proposed DC–DC converter is shown in Fig. 3. The primary side has a boost converter and pulse-width modulation (PWM) switching voltages controlled by a single main switch. The secondary side has an isolated charge pump. Both outputs are serially connected, which can be called a *stacked-output*. The single-ended structure of the proposed converter is suitable for small power capacity. Compared with other bridge-type topologies, a single-ended structure has discontinuous conduction mode (DCM) with low current capacity over high output voltage. The DCM can eliminate the reverse-recovery of the diode.

We analyze the steady-state input–output transfer gain of the proposed converter. Fig. 4 shows that the charge pump and boost converter can be analyzed by output separation by using an equivalent circuit transformation. Both output

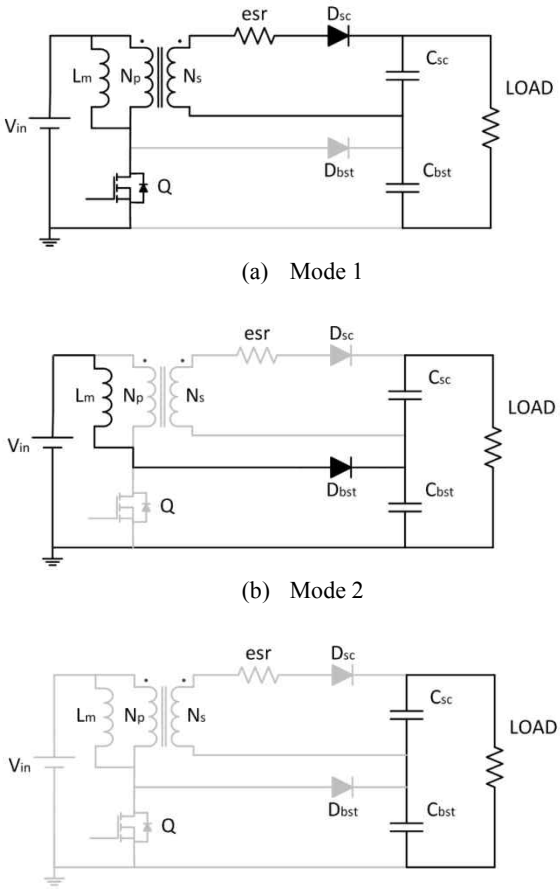


(a) Mode 1

(b) Mode 2

(c) Mode 3

Fig. 5. Equivalent circuits of each operation mode.

currents ($I_{O\_cp}$) and ($I_{O\_bst}$) are the same because of the series connection in a series-connected switched-capacitor boost (SSCB) converter. Equation (2) indicates each of the load resistances for the equivalent transformation.

$$R_{sc} = \frac{V_{o\_sc}}{I_{Load}}, \quad R_{bst} = \frac{V_{o\_bst}}{I_{Load}} \tag{2}$$

As aforementioned, the steady-state voltage gain of the isolated switched capacitor cell is determined only by the turns ratio of the winding of the transformer.

$$M_{VDC\_sc} = \frac{V_{o\_sc}}{V_{in}} = \frac{N_s}{N_p} \tag{3}$$

The steady-state voltage gain of the DCM boost is derived as follows:

$$M_{VDC\_bst} = \frac{1}{2}\left(1 + \sqrt{1 + \frac{2D^2 R_{bst} T}{L_m}}\right), \tag{4}$$

where $T$ is the switching period, and $D$ is the duty cycle. Each parameter of the derivation is denoted in Fig. 4.

The final input–output transfer function of the SSCB converter is derived from the equivalent transformation in DCM. The final input–output transfer function can be expressed as

$$M_{VDC} = M_{VDC_{sc}} + M_{VDC_{bst}} = \frac{N_s}{N_p} + \frac{1}{2}\left(1 + \sqrt{1 + \frac{2D^2 R_{bst} T}{L_m}}\right). \tag{5}$$

### B. Operating Principles

According to the switching state of the switching circuits, the proposed converter has three operating modes (see Fig. 5).

Mode 1: When the switch ($Q$) is turned on, the current flows to the magnetizing inductance and the primary winding ($N_p$). The primary current is transferred to the secondary ($N_s$) coil of the isolated switched capacitor cell via the magnetic linkage. Through the switched capacitor diode $D_{sc}$, the secondary current is rectified into DC as the load requires. Given that the boost diode ($D_{bst}$) is reverse-biased, the output capacitor $C_{sc}$ discharges the load current.

Mode 2: When the switch $Q$ is turned off, the switched capacitor diode ($D_{sc}$) is reverse-biased. The energy magnetically stored at $L_m$ is released to the load through $D_{bst}$ of the boost converter. When the switched capacitor diode ($D_{sc}$) is reverse biased, the output capacitor $C_{bst}$ discharges the load current.

Mode 3: The transformer of the charge pump-boost converter is completely demagnetized. The output voltage is also maintained by the discharge of the output capacitors $C_{sc}$, $C_{bst}$. All rectifier diodes are reverse-biased.

The key waveforms of the operating voltage and current are shown in Fig. 10.

## IV. Power Loss Analysis of the SSCB Converter

For the efficiency prediction, the key parameters such as the input current and switch current of the SSCB converter can be derived as follows:

The turn-ratio is expressed as

$$n = \frac{N_s}{N_p}. \tag{6}$$

The input peak and average current are given by

$$I_{in\_pk} = \frac{nI_o(1-D)T}{R_{esr}C\left(1-e^{-\frac{DT}{\tau}}\right)} + nI_o \tag{7}$$

$$I_{in\_avg} = \frac{P}{V_{in}} = \frac{(I_{in\_pk} + I_{in\_DT})D + I_{Lm\_max}}{2}. \tag{8}$$

The magnetizing current is given by

$$I_{Lm\_max} = \frac{V_{in} DT}{L_m}. \tag{9}$$

The average input current is expressed as

$$I_{in\_DT} = \frac{2P}{DV_{in}} - \frac{nI_o(1-D)T}{R_{esr}C\left(1-e^{-\frac{DT}{\tau}}\right)} - nI_o - \frac{V_{in}T}{L_m}. \tag{10}$$

The on-time current is expressed as

$$i_{in\ (t:0\sim DT)} = \frac{-(I_{in\_pk}-I_{in\_DT})}{DT}t + I_{in\_pk} \quad . \tag{11}$$

The off-time current is given by

$$i_{in\ (t:DT\sim(D+D_1)T)} = \frac{V_{in}\left(-\frac{D}{D_1}\right)}{L_m}t + \frac{V_{in}\left(\frac{D+D_1}{D_1}\right)}{L_m}DT \quad . \tag{12}$$

The diode off-time current is expressed as

$$i_{in\ (t:DT\sim T)} = 0 \quad . \tag{13}$$

The RMS input current is expressed as

$$i_{in\ (t)_{rms}} = \sqrt{\frac{1}{T}\left(\int_0^{DT} {i_{in\ (t:0\sim DT)}}^2 dt + \int_{DT}^{(D+D_1)T} {i_{in\ (t:DT\sim(D+D_1)T)}}^2 dt\right)} = \sqrt{\frac{D}{3}\left({I_{in\_pk}}^2 + I_{in\_pk}I_{in\_DT} + {I_{in\_DT}}^2\right) + \frac{{V_{in}}^2 D^2 T^2}{{L_m}^2 {D_1}^2}\left(\frac{{D_1}^3}{3}\right)} \quad . \tag{14}$$

*A. MOSFET*

The conduction loss is as follows:

$$P_{Q\_con} = r_{DS}{I_{Q\_rms}}^2, \tag{15}$$

where,

$$I_{Q\_rms} = \sqrt{\frac{1}{T}\int_0^{DT} {i_{in\ (t:0\sim DT)}}^2 dt} = \sqrt{\frac{D}{3}\left({I_{in\_pk}}^2 + I_{in\_pk}I_{DT} + {I_{in\_DT}}^2\right)}. \tag{16}$$

The conduction loss is given by

$$P_{Q\_con} = \frac{RQD}{3}\left({I_{in\_pk}}^2 + I_{in\_pk}I_{DT} + {I_{in\_DT}}^2\right). \tag{17}$$

The switching loss is as follows:

$$P_{Q\_sw} = \frac{f_s C_o {V_{ds}}^2}{2}. \tag{18}$$

The total loss is given by

$$P_Q = \frac{R_Q D}{3}\left({I_{in\_pk}}^2 + I_{in\_pk}I_{DT} + {I_{in\_DT}}^2\right) + \frac{f_s C_o {V_{ds}}^2}{2} \quad .(19)$$

*B. Diode*

The loss of $D_{sc}$ can be derived as follows:

The average and RMS current are given by

$$I_{sc} = \frac{1}{T}\int_0^{DT} i_{D\_sc}\, dt = I_o \tag{20}$$

$$I_{D_{sc}\_rms} = \sqrt{\frac{1}{nT}\int_0^{DT} {i_{in\ (t:0\sim DT)}}^2 dt} \quad . \tag{21}$$

The conduction loss can be derived from the forward drop loss and the resistive loss. The conduction loss can be expressed as

$$P_{D_{sc}\_VF} = V_F I_{D\_sc} = V_F I_o, \tag{22}$$

and the resistive loss term can be expressed as

$$P_{D_{sc}\_RF} = R_F {I_{D_{sc}\_rms}}^2 = \frac{R_F D}{3n}\left({I_{in\_pk}}^2 + I_{in\_pk}I_{DT} + {I_{in\_DT}}^2\right) \quad . \tag{23}$$

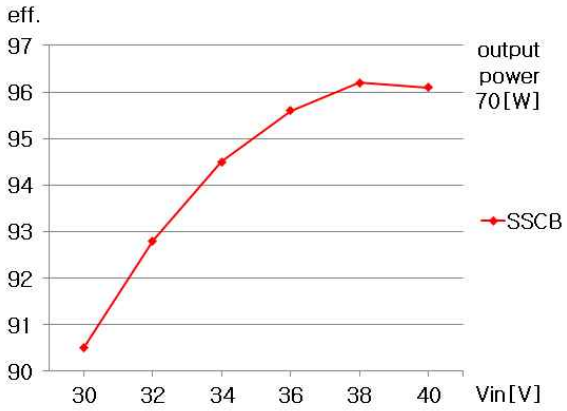


Fig. 6. Simulation result of the SSCB converter according to the variation of the input voltage.

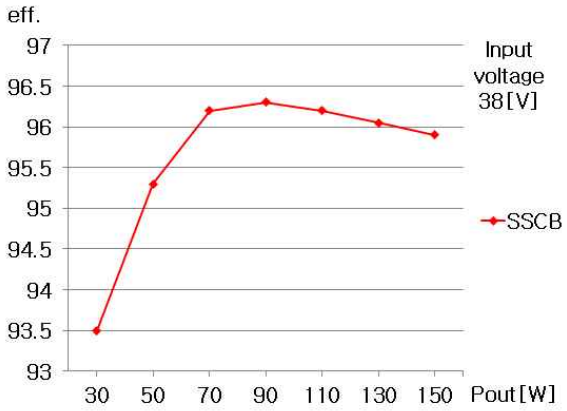


Fig. 7. Simulation result of the SSCB converter according to the variation of the output power.

The total loss is

$$P_{D_{sc}} = \frac{R_F D}{3n}\left({I_{in\_pk}}^2 + I_{in\_pk}I_{DT} + {I_{in\_DT}}^2\right) + V_F I_o. \tag{24}$$

The loss of $D_{bst}$ can be derived as follows.

The average and RMS current are

$$I_{D_{bst}} = \frac{1}{T}\int_{DT}^{(D+D_1)T} i_{D\_bst}\, dt = I_o \tag{25}$$

$$I_{D_{bst}\_rms} = \sqrt{\frac{1}{T}\int_{DT}^{(D+D_1)T} {i_{in\ (t:DT\sim(D+D_1)T)}}^2 dt} \quad . \tag{26}$$

The conduction loss can be derived from the forward drop loss and the resistive loss. The conduction loss can be expressed as follows:

$$P_{D_{bst}\_VF} = V_F I_{D\_bst} = V_F I_o. \tag{27}$$

The resistive loss term is

$$P_{D_{bst}\_RF} = R_F {I_{D_{bst}\_rms}}^2 = \frac{R_F {V_{in}}^2 D^2 T^2}{{L_m}^2 {D_1}^2}\left(\frac{{D_1}^3}{3}\right) \quad . \tag{28}$$

The total loss is

$$P_{D_{bst}} = \frac{R_F {V_{in}}^2 D^2 T^2}{{L_m}^2 {D_1}^2}\left(\frac{{D_1}^3}{3}\right) + V_F I_o. \tag{29}$$

*C. Transformer*

The primary winding loss of the transformer can be expressed as follows:

$$P_{Tr\_N_p} = R_{N_p} I_{N_p\_rms}{}^2 \quad , \tag{30}$$

where,

$$R_{N_{esr}} = \frac{\rho \cdot n(MLT)}{A_\omega}[\Omega] \tag{31}$$

$\rho$: wire resistivity , $n$: wire turns ,

$MLT$: Mean Length per Turn , $A_\omega$: wire size $[cm^2]$

and

$$I_{N_{p_{rms}}} = i_{in\,(t)_{rms}} = \sqrt{\frac{1}{T}\left(\int_0^{DT} i_{in\,(t:0\sim DT)}{}^2 dt + \int_{DT}^{(D+D_1)T} i_{in\,(t:DT\sim(D+D_1)T)}{}^2 dt\right)} = \sqrt{\frac{D}{3}\left(I_{in\_pk}{}^2 + I_{in\_pk} I_{in\_DT} + I_{in\_DT}{}^2\right) + \frac{V_{in}{}^2 D^2 T^2}{L_m{}^2 D_1{}^2}\left(\frac{D_1{}^3}{3}\right)}. \tag{32}$$

Therefore, the primary winding loss can be re-written as follows:

$$P_{Tr\_N_p} = R_{N_p}\{\frac{D}{3}\left(I_{in_{pk}}{}^2 + I_{in_{pk}} I_{in_{DT}} + I_{in_{DT}}{}^2\right) + \frac{V_{in}{}^2 D^2 T^2}{L_m{}^2 D_1{}^2}\left(\frac{D_1{}^3}{3}\right)\}. \tag{33}$$

The secondary winding loss of the transformer is

$$P_{Tr\_N_s} = R_{N_s} I_{N_s\_rms}{}^2, \tag{34}$$

where,

$$I_{N_{s_{rms}}} = I_{D_{sc}\_rms}. \tag{35}$$

Therefore, the secondary winding loss of the transformer can be re-written as follows:

$$P_{Tr\_N_s} = \frac{R_{N_s} D}{3n}\left(I_{in\_pk}{}^2 + I_{in\_pk} I_{DT} + I_{in\_DT}{}^2\right). \tag{36}$$

The energy loss of the transformer core is

$$W_{Tr_{\text{hys}}} = \int v(t) i(t) dt = \int \left(nA_c \frac{dB(t)}{dt}\right)\left(\frac{H(t)L_m}{n}\right) dt = A_c L_m \int H\,dB\,[J].$$

The power loss is

$$P_{Tr_{\text{hys}}} = f_s A_c L_m \int H\,dB\,[W] \quad . \tag{37}$$

*D. Simulation Results*

The simulation results of the efficiency analysis for the SSCB converter according to the output power variation and input voltage are shown in Figures 6 and 7, respectively. Results show that the efficiency is high and is even greater than 96% in low-gain (high-input) conditions. The efficiency significantly drops when the voltage gain is out of the boost boundary in the low input range.

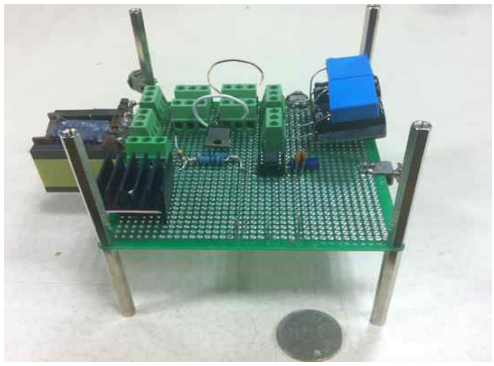

Fig. 8. Photograph of the hardware prototype of the proposed SSCB converter.


Fig. 9. Photograph of the experimental setup.

TABLE I

KEY PARAMETER OF SERIES-OUTPUT ISOLATED-SWITCHED-CAPACITOR BOOST CONVERTER HARDWARE

| Symbol | Parameter(part number) | Spec. |
|---|---|---|
| $V_{in}$ | Input voltage | 30 $V_{DC}$ to 40 $V_{DC}$ |
| $V_{out}$ | Output voltage | 340 $V_{DC}$ |
| $P_{out}$ | Output power | 30 W to 150 W |
| $f_s$ | Switching frequency | 40 kHz |
| $L_m$ | Magnetizing inductance | 440 uH |
| Q | Main switch (IRFP260N) | 200 V, 50 A |
| $N_p$ | Primary winding | 13 turns |
| $N_s$ | Secondary winding | 91 turns |
| $D_{sc}$ | Diode of switched capacitor (UF4006) | 800 V, 1 A |
| $D_{bst}$ | Boost's diode(UF4004) | 400 V, 1 A |

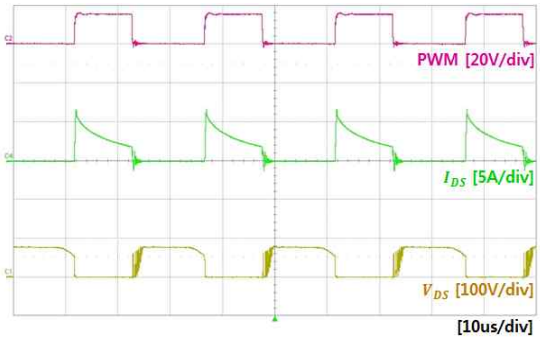


(a) $I_{DS}$: MOSFET drain current, $V_{DS}$: MOSFET drain-source voltage.

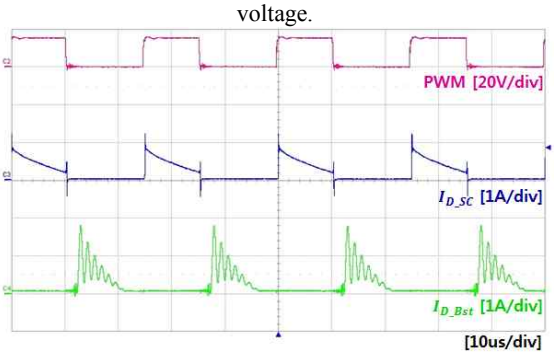


(b) $I_{D\_SC}$: Current of the switched capacitor rectifier, $I_{D\_bst}$: current of the boost rectifier.

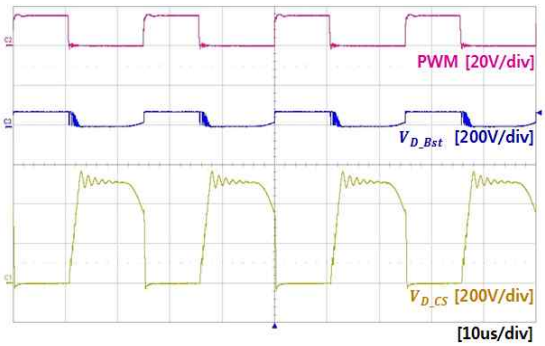


(c) $V_{D\_bst}$: Boost's diode voltage, $V_{D\_SC}$: Switched capacitor's diode voltage.

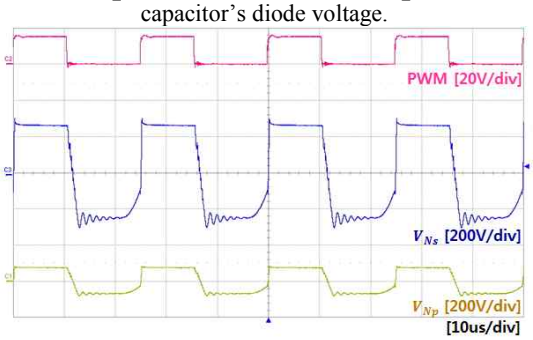


(d) $V_{Np}$: Primary winding voltage, $V_{Ns}$: Secondary winding voltage.

Fig. 10. Key waveforms of the hardware experiment.

## V. Experimental Validation

In this paper, a 150W hardware prototype of the proposed SSCB PWM converter was implemented to verify the operation principles and converter performance. The implemented component data concerning the prototype are listed in Table I. The prototype pictures and experimental set up are presented in Fig. 8 and 9.

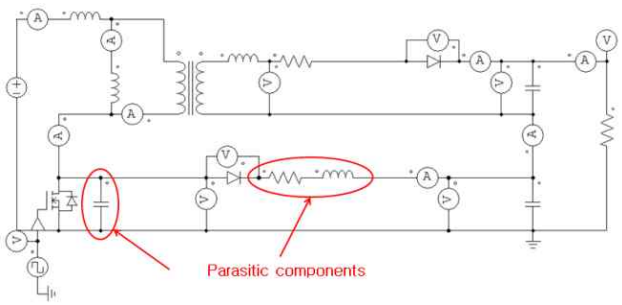


Fig. 11. Parasitic components of the SSCB converter.

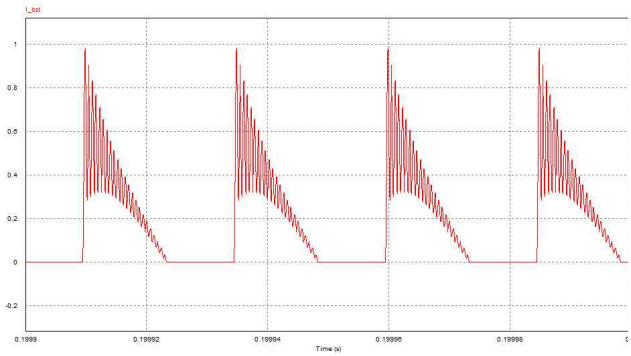

Fig. 12. Simulation result of $I_{D_{bst}}$ waveform with the parasitic components in Fig. 11.

Fig. 10(a) shows the waveforms of the PWM gate signal, the drain-source voltage of the MOSFET, and the switch current without a snubber. Fig. 10(b) shows the waveforms of the current of $D_{sc}$ and $D_{bst}$. The boost output operates in DCM. The ringing of the current occurs due to the parasitic capacitance of the MOSFET and the parasitic inductor of the boost circuit. Fig. 10(c) and 10(d) show the voltage waveforms of the diodes and transformer winding,

respectively. All the figures match well with the operating principles presented in Section III. Fig. 11 shows the parasitic components of the SSCB converter, which caused the ringing of $I_{D_{bst}}$ current. A parasitic inductance existing on the wire between the diode and the output capacitor resonates with a parasitic capacitance of the MOSFET. The simulation waveform of $I_{D_{bst}}$ current is shown in Fig. 12. The parasitic components caused the current ringing during the diode conduction.

Fig. 13 shows the efficiency of the efficiency measurement according to the input voltage and output power variation. Experiment results show that the efficiency is high and is even greater than 96% in low-gain (high-input) conditions. The efficiency significantly drops when the voltage gain is out of the boost boundary in the low input range. Compared with the analysis results in Fig. 6 and 7, the

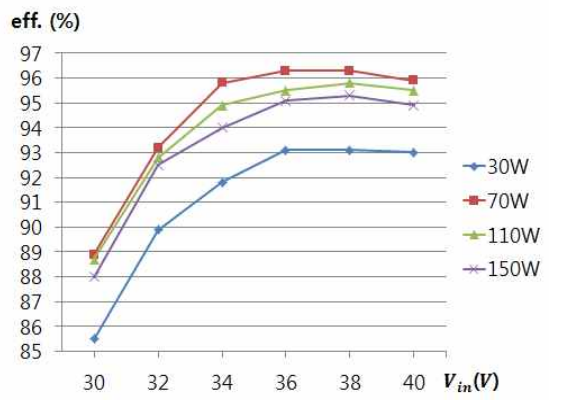


Fig. 13. Power efficiency of the proposed SBSC converter according to the variation of output power.

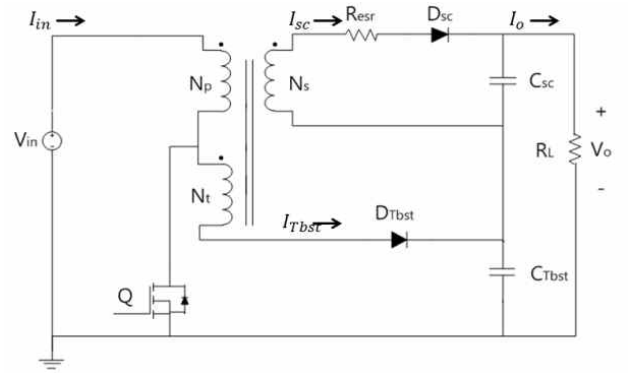


Fig. 14. Circuit diagram of the proposed SCTI converter.

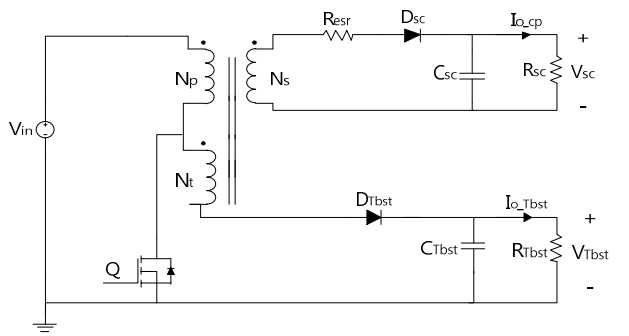


Fig. 15. Equivalent circuit of the proposed converter with separated outputs.

prototype hardware operates similarly to the theoretical principles.

To improve more, another version is provided. Fig. 14 shows the structure of the proposed DC–DC converter, named as 'isolated switched-capacitor tapped-inductor (SCTI) boost converter'. The proposed converter consists of two parts. The primary side has a TI boost converter with a single main switch controlled by a PWM compensator and a gate-driver. The secondary side has an isolated charge pump. From the inductor tapping, the main switch voltage stress is reduced, and the voltage spike on the switch is significantly attenuated. Given that low voltage stress exists on the active switch, the circuits can use low voltage MOSFETs, which generally have low *R*ds(on). MOSFETs decrease the conduction loss dramatically [10], thus making this variable one of the dominant factors of efficiency. The output of the switched cell is connected with the boost output in series. The stacked-output structure of the proposed converter is suitable for high-voltage and low-current applications. Compared with other multiple-module connected topologies, MOSFET and diode are relieved from severe voltage stress. The DCM is also employed to eliminate the reverse-recovery loss of the diode.

## VI. ISOLATED SWITCHED-CAPACITOR TAPPED-INDUCTOR BOOST CONVERTER

### *A. Structure of the Proposed Converter*

To analyze the input–output voltage gain of the proposed converter in a steady-state condition, the TI boost converter and charge-pump outputs are separated equivalently (Figure 15). Both of the boost output current ($I_{o\_Tbst}$) and charge pump output current ($I_{o\_cp}$) are similar because of the series-connected output. Equation (38) indicates each of the load resistances for the equivalent transformation.

$$R_{sc} = \frac{V_{sc}}{I_{Load}} \quad , \quad R_{Tbst} = \frac{V_{Tbst}}{I_{Load}} \tag{38}$$

As shown in (39), the voltage gain of the isolated switched capacitor is determined by the turn ratio of the winding of the transformer in steady-state condition.

$$M_{VDC\_sc} = \frac{V_{sc}}{V_{in}} = \frac{N_s}{N_p} \tag{39}$$

The steady-state voltage gain of the DCM tapped-inductor boost is derived as follows:

$$M_{VDC\_Tbst} = \frac{1}{2}\left(1 + \sqrt{1 + \frac{2D^2 R_{Tbst} T}{L_m}}\right). \tag{40}$$

Thus, the input–output voltage gain of the proposed converter is derived from the equivalent circuit in DCM. The input–output voltage can be expressed as follows:

$$M_{VDC} = M_{VDC\_Tbst} + M_{VDC\_sc} \tag{41}$$

$$M_{VDC} = \frac{N_s}{N_p} + \frac{1}{2}\left(1 + \sqrt{1 + \frac{2D^2 R_{Tbst} T}{L_m}}\right). \tag{42}$$

### *B. Operating Principle*

The proposed converter has three operating modes. Fig. 16 shows the equivalent circuits to explain the circuit operation.

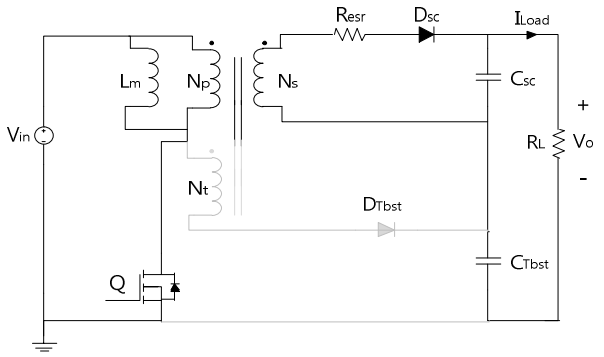


(a) Mode 1.

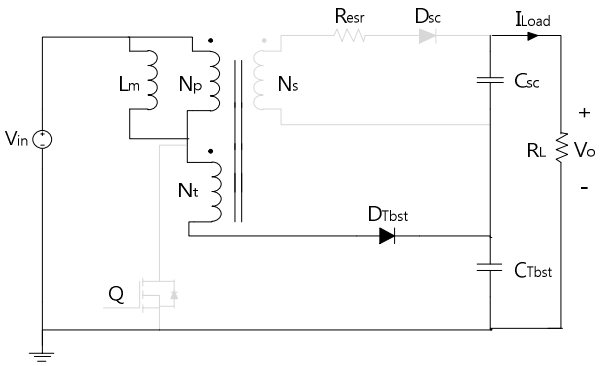


(b) Mode 2.

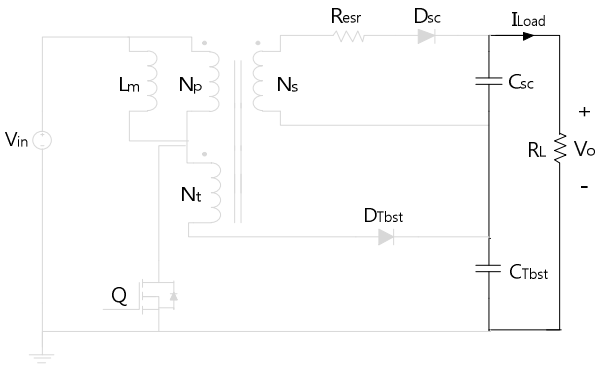


(c) Mode 3.

Fig. 16. Operating modes of the proposed converter.

Mode 1: When the main switch $Q$ closes, the input current flows to the magnetizing inductance ($L_m$) and primary winding ($N_p$). The primary current and voltage are transferred as secondary ($N_s$) coil through flux linkage. The capacitor diode ($D_{sc}$) is turned on. As a load requirement through the switched capacitor diode ($D_{sc}$) and output capacitor ($C_{sc}$), the secondary current is then rectified into DC. The TI boost converter diode ($D_{Tbst}$) is turned off when the main switch turns on. In this mode, the TI output capacitor ($C_{Tbst}$) discharges the load current to fix the output voltage.

Mode 2: The main switch $Q$ turns off. The switched capacitor diode ($D_{sc}$) is reverse-biased and is turned off. The tapped-inductor boost converter diode ($D_{Tbst}$) becomes forward-biased when the main switch turns off. The magnetic energy stored in $L_m$ is provided to the tapped boost output capacitor ($C_{Tbst}$) through $D_{Tbst}$ of the TI boost converter. The output capacitor ($C_{sc}$) discharges the load current to fix the output voltage.

Mode 3: All magnetizing components in the transformer and TI are completely de-magnetized. The output voltage is fixed by both output capacitors $C_{sc}$, $C_{Tbst}$ discharge.

## VII. Power Loss Analysis of SCTI Converter

The key parameters of the SCTI converter are derived as follows:

The turn-ratios are expressed as

$$n = \frac{N_s}{N_p}, \quad n_{TI} = \frac{N_p + N_t}{N_p}. \tag{43}$$

The turn-on time diode current is given by

$$I_{sc\_0} = \frac{I_o(1-D)T}{R_{esr}\, C\left(1-e^{-\frac{DT}{\tau}}\right)} + I_o \ . \tag{44}$$

The average current is given by

$$I_{sc\_avg} = I_o = \frac{(I_{sc\_0} + I_{sc\_DT})D}{2} \ . \tag{45}$$

The turn-off current is given by

$$I_{sc\_DT} = \frac{I_o(2-D)}{D} - \frac{I_o(1-D)T}{R_{esr}\, C\left(1-e^{-\frac{DT}{\tau}}\right)}. \tag{46}$$

Therefore, the turn-on time input current is given by

$$I_{in\_0} = nI_{sc\_0} \ . \tag{47}$$

The turn-off current is expressed as

$$I_{in\_DT} = nI_{sc\_DT} + I_{L_m\_max} \ . \tag{48}$$

where,

$$I_{L_m\_max} = \frac{V_{in}\, DT}{L_m}. \tag{49}$$

The on-time current is given by

$$i_{in\ (t:0\sim DT)} = \frac{(I_{in\_DT} - I_{in\_0})}{DT} t + I_{in\_0} \tag{50}$$

The off-time current is expressed as

$$i_{in\ (t:DT\sim(D+D_1)T)} = \frac{V_{in}\left(-\frac{D}{D_1}\right)}{n_{TI} L_m} t + \frac{V_{in}\left(\frac{D+D_1}{D_1}\right)}{n_{TI} L_m} DT \tag{51}$$

Finally, the diode-off time current is given by

$$i_{in\ (t:(D+D_1)T\sim T)} = 0. \tag{52}$$

The RMS input current is

$$i_{in\ (t)rms} = \sqrt{\frac{1}{T}\left(\int_0^{DT} {i_{in\ (t:0\sim DT)}}^2 dt + \int_{DT}^{(D+D_1)T} {i_{in\ (t:DT\sim(D+D_1)T)}}^2 dt\right)} = \sqrt{\frac{D}{3}\left({I_{in\_0}}^2 + I_{in\_0} I_{in\_DT} + {I_{in\_DT}}^2\right) + \frac{{V_{in}}^2 D^2 T^2}{n_{TI} {L_m}^2 {D_1}^2}\left(\frac{{D_1}^3}{3}\right)}. \tag{53}$$

### A. MOSFET

The conduction loss can be derived as follows:

$$P_{Q\_con} = r_{DS} I_{Q\_rms}^2 \quad (54)$$

where,

$$I_{Q\_rms} = \sqrt{\frac{1}{T}\int_0^{DT} i_{in\ (t:0\sim DT)}^2 dt} = \sqrt{\frac{D}{3}\left(I_{in\_0}^2 + I_{in\_0} I_{DT} + I_{in\_DT}^2\right)} \quad (55)$$

Then, the conduction loss is

$$P_{Q\_con} = \frac{RQD}{3}\left(I_{in\_0}^2 + I_{in\_0} I_{DT} + I_{in\_DT}^2\right) \quad (56)$$

The switching loss is as follows:

$$P_{Q\_sw} = \frac{f_s C_o V_{ds}^2}{2}. \quad (57)$$

The total loss is

$$P_Q = \frac{R_Q D}{3}\left(I_{in\_0}^2 + I_{in\_0} I_{DT} + I_{in\_DT}^2\right) + \frac{f_s C_o V_{ds}^2}{2}. \quad (58)$$

The switch on, off time loss can be ignored by the DCM operation

*B. Diode*

The loss of $D_{sc}$ can be derived as follows:

The average and RMS current are

$$I_{sc} = \frac{1}{T}\int_0^{DT} i_{D\_sc}\, dt = I_o \quad (59)$$

$$I_{D_{sc}\_rms} = \sqrt{\frac{1}{nT}\int_0^{DT} i_{in\ (t:0\sim DT)}^2 dt}. \quad (60)$$

The conduction loss can be derived from the forward drop loss and the resistive loss. The conduction loss can be expressed as follows:

$$P_{D_{sc}\_VF} = V_F I_{D\_sc} = V_F I_o \ , \quad (61)$$

and the resistive loss term is

$$P_{D_{sc}\_RF} = R_F I_{D_{sc}\_rms}^2 = \frac{R_F D}{3n}\left(I_{in\_pk}^2 + I_{in\_pk} I_{DT} + I_{in\_DT}^2\right). \quad (62)$$

The total loss is

$$P_{D_{sc}} = \frac{R_F D}{3n}\left(I_{in\_pk}^2 + I_{in\_pk} I_{DT} + I_{in\_DT}^2\right) + V_F I_o. \quad (63)$$

The loss of $D_{Tbst}$ can be derived as follows:

The average and RMS current are

$$I_{D_{Tbst}} = \frac{1}{T}\int_{DT}^{(D+D_1)T} i_{D\_Tbst}\, dt = I_o \quad (64)$$

$$I_{D_{Tbst}\_rms} = \sqrt{\frac{1}{T}\int_{DT}^{(D+D_1)T} i_{in\ (t:DT\sim(D+D_1)T)}^2 dt}. \quad (65)$$

The conduction loss can be derived from the forward drop loss and the resistive loss. The conduction loss can be expressed as follows:

$$P_{D_{Tbst}\_VF} = V_F I_{D\_Tbst} = V_F I_o, \quad (66)$$

and the resistive part of diode conduction loss is

$$P_{D_{Tbst}\_RF} = R_F I_{D_{Tbst}\_rms}^2 = \frac{R_F V_{in}^2 D^2 T^2}{n_{TI} L_m^2 D_1^2}\left(\frac{D_1^3}{3}\right). \quad (67)$$

Therefore, the total loss is

TABLE II
KEY PARAMETERS OF THE PROPOSED CONVERTER

| Symbol | Parameter(part number) | Spec. |
|---|---|---|
| $V_{in}$ | Input voltage | 20 – 40 $V_{DC}$ |
| $V_{out}$ | Output voltage | 340 $V_{DC}$ |
| $P_{out}$ | Output power | 40 – 100 W |
| $f_s$ | Switching frequency | 35 kHz |
| $L_m$ | Magnetizing inductance | 108 uH |
| Q | Main switch (IRFP4468) | 100 V, 195 A |
| $N_p$ | Primary winding | 14 turns |
| $N_s$ | Secondary winding(Transformer) | 70 turns |
| $N_t$ | Third winding(Tapped-inductor) | 42 turns |
| $D_{sc}$ | Switched capacitor diode(MBR40250) | 250 V, 40 A |
| $D_{Tbst}$ | TI boost diode(UF4004) | 400 V, 1 A |
| $C_{sc}$, $C_{Tbst}$ | capacitance | 100μF |

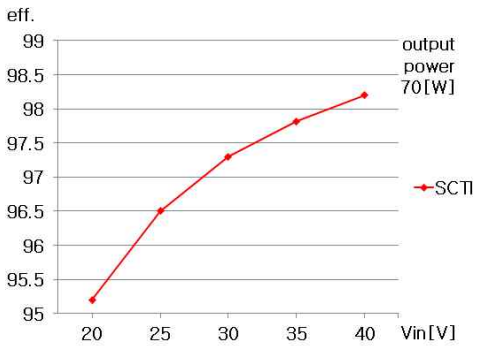


Fig. 17. Simulation result of the MATLAB Simulink according to the variation of the input voltage.

$$P_{D_{Tbst}} = \frac{R_F V_{in}^2 D^2 T^2}{n_{TI} L_m^2 D_1^2}\left(\frac{D_1^3}{3}\right) + V_F I_o. \quad (68)$$

*C. Transformer*

The primary winding loss of the transformer can be expressed as follows:

$$P_{Tr\_N_p} = R_{N_p} I_{N_p\_rms}^2, \quad (69)$$

where,

$$I_{N_p\_rms} = i_{in\ (t)\_rms} = \sqrt{\frac{1}{T}\left(\int_0^{DT} i_{in\ (t:0\sim DT)}^2 dt + \int_{DT}^{(D+D_1)T} i_{in\ (t:DT\sim(D+D_1)T)}^2 dt\right)} = \sqrt{\frac{D}{3}\left(I_{in\_0}^2 + I_{in\_0} I_{in\_DT} + I_{in\_DT}^2\right) + \frac{V_{in}^2 D^2 T^2}{n_{TI} L_m^2 D_1^2}\left(\frac{D_1^3}{3}\right)}. \quad (70)$$

Therefore, the primary winding loss can be rewritten as follows:

$$P_{Tr\_N_p} = R_{N_p}\{\frac{D}{3}\left(I_{in_0}{}^2 + I_{in_0}I_{in_{DT}} + I_{in_{DT}}{}^2\right) + \frac{V_{in}{}^2D^2T^2}{n_{TI}L_m{}^2D_1{}^2}\left(\frac{D_1{}^3}{3}\right)\}. \quad (71)$$

The secondary winding loss of the transformer is

$$P_{Tr\_N_s} = R_{N_s}I_{N_s\_rms}{}^2, \quad (72)$$

where,

$$I_{N_{s_{rms}}} = I_{D_{sc}\_rms}. \quad (73)$$

The secondary winding loss of the transformer can be rewritten as follows:

$$P_{Tr\_N_s} = \frac{R_{N_s}D}{3n}\left(I_{in\_0}{}^2 + I_{in\_0}I_{DT} + I_{in\_DT}{}^2\right). \quad (74)$$

The tertiary winding loss of the transformer is

$$P_{Tr\_N_t} = R_{N_t}I_{N_t\_rms}{}^2, \quad (75)$$

where,

$$I_{N_{s_{rms}}} = I_{D_{Tbst}\_rms}. \quad (76)$$

The tertiary winding loss of the transformer can be re-written as follows:

$$P_{Tr\_N_t} = \frac{R_{N_t}V_{in}{}^2D^2T^2}{n_{TI}L_m{}^2D_1{}^2}\left(\frac{D_1{}^3}{3}\right). \quad (77)$$

The core loss of the transformer is derived the same as in Section IV.

*D. Simulation results*

Fig. 17 shows a simulation analysis result of the conversion efficiency for the proposed converter according to the input voltage variation. As shown in Fig. 17, the maximum efficiency is supposed to be higher than 98% at 40 V. However, the efficiency decreases as the input voltage decreases.

## VIII. EXPERIMENTAL RESULTS

In this paper, a 100W hardware prototype of the proposed PWM converter was implemented to verify the operation principles and the performance of the converter. The implemented component data concerning the hardware prototype are listed in Table II.

Fig. 18(a) shows the waveforms of the PWM gate signal, the drain-source voltage of MOSFETs without a snubber, and the input current. Fig. 18(b) shows the waveforms of the boost diode and the capacitor. The boost output operates in DCM. Fig. 18(c) and 18(d) show the current and voltage waveforms of the diodes, respectively. All figures match well with the operating principles presented in Section VI.

Fig. 19 shows the hardware efficiency of the proposed converter. The efficiency graph shows the measurement data according to the input voltage and load power variation. As shown in Fig. 19, the maximum efficiency is higher than 98% at 40V. However, the efficiency is reduced as the input voltage decreases or as the output power approaches full load.

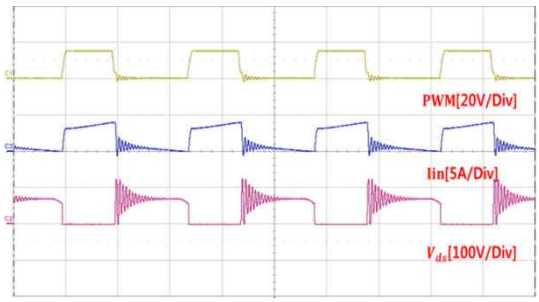


(a) $I_{in}$: Input current, $V_{DS}$: MOSFET drain-source voltage

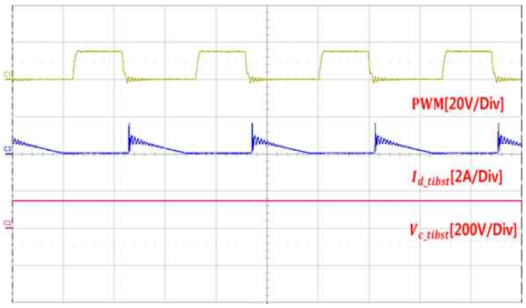


(b) $I_{d\_tbst}$ : Tapped-Inductor Boost Converter Diode current, $V_{c\_tbst}$ : Tapped-Inductor Boost Converter capacitor voltage.

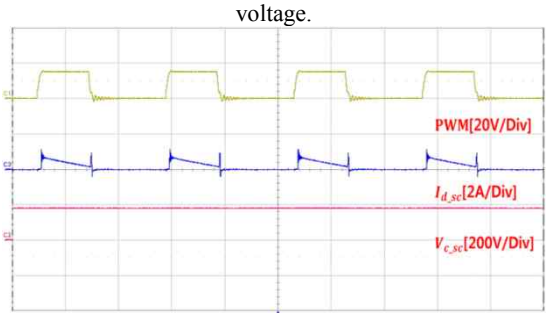


(c) $I_{d\_sc}$ : Switched capacitor rectifier's current, $V_{c\_sc}$ : Switched capacitor voltage.

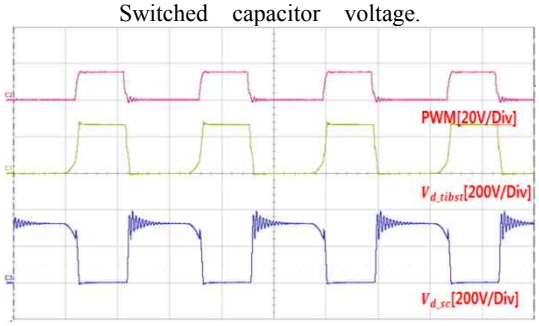


(d) $V_{d\_tbst}$ : Tapped-Inductor Boost Converter Diode Voltage, $V_{d\_sc}$: Switched capacitor Diode voltage

Fig. 18. Key waveforms of the hardware experiment.

Compared with the analysis results in Fig. 17, the prototype hardware operates similarly to the theoretical principles. The power efficiency of the SCTI converter is also compared with a conventional series-connected forward-flyback converter (SFFB) in Fig. 20. The power efficiency of the SCTI converter is greater than that of the SFFB converter [1] in the entire range.

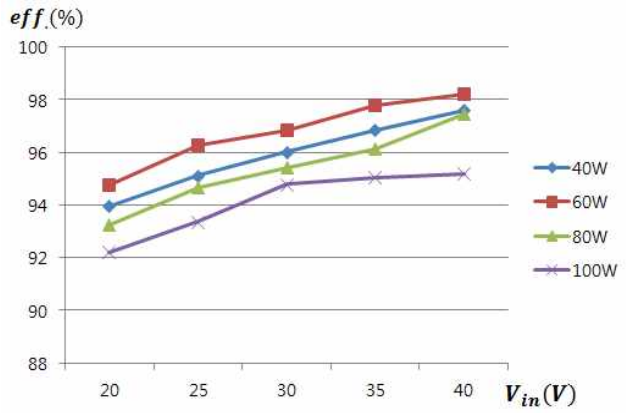


Fig. 19. Efficiency measurement graph of the proposed converter.

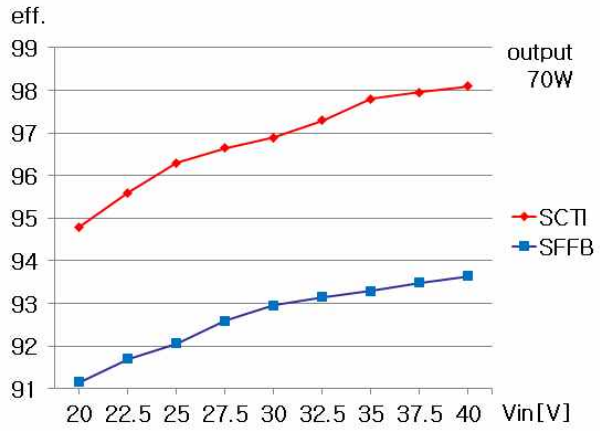


Fig. 20. Comparison of power efficiency.

## IX. CONCLUSIONS

In this paper, we proposed a pre-regulating DC–DC converter, specifically a series-connected isolated-switched-capacitor boost converter, for multi-stage PV power conditioning systems. The single-ended charge-pump-boost operation, which contributes to the high-density power delivery of the transformer, is beneficial to the enhancement of the output voltage with low cost. The high-voltage and low-current output have a filter inductor under DCM operation. The filter conductor contributes to the better performance of the DCM by eliminating reverse recovery of the rectifying diodes. The operational principle of the boost-isolated switched capacitor converter has been presented by obtaining the equivalent transformation from load-sharing ratio in series output. The experimental result of the 150W hardware prototype is included to show that the proposed converter has high efficiency, which is greater than 96% of the middle range of 30 V to 40 V input to 340V output.

We also presented another novel high step-up series-connected and isolated switched-capacitor boost converter that employs a TI. The TI allows extreme step-up voltage while maintaining a moderate duty ratio. The switching component stresses decrease with the application of an isolated switched capacitor cell. All sub-converters are integrated with a single switch and a single magnetic device. This integration results in the increase in converter efficiency with minimum extra cost. The experimental results of a 100 W hardware prototype verify the performance and efficiency of the proposed converter.

## ACKNOWLEDGEMENT

This work was supported by the Human Resources Development Program(No. 20124010203160) of the KETEP funded by the Korea government Ministry of Trade, Industry and Energy and by the Basic Science Research Program through the National Research Foundation of Korea funded by the Ministry of Education, Science and Technology under Grant 2012-0006984.

## REFERENCES

[1] J. H. Lee, J. H. Park, and J. H. Jeon, "Series-connected forward-flyback converter for high step-up power conversion," *IEEE Trans. Power Electron.*, Vol. 26, No. 12, pp. 3629-3641, Dec. 2011.

[2] K. B. Park, G. W. Moon, and M. J. Youn, "High step-up boost converter intergrated with a transformer-assisted auxilary circuit employing quasi-resonant operation," *IEEE Trans. Power Electron.*, Vol. 27, No. 6, pp. 1974-1984, Apr. 2012.

[3] S. K. Changchien, T. J. Liang, and J. F. Chen, "Novel high step-up DC-DC converter for fuel cell energy conversion system", *IEEE Trans. Ind. Electron.*, Vol. 57, No. 6, pp. 2007-2017, Jun. 2010.

[4] K. Zou, Scott, M. J., Jin Wnag "A switched-capacitor voltage tripler with automatic interleaving capability," *IEEE Trans. Power Electron.*, Vol. 27, No. 6, pp2857-2868, Jun. 2012.

[5] S. Jiang, D. Cao, Y. Li, and F. Z. Peng, "Grid-connected boost-half-bridge photovoltaic microinverter system using repetitive current control and maximum power point tracking," *IEEE Trans. Power Electron*, Vol. 27, No. 11, pp.4711-4722, Nov. 2012.

[6] F. H. Dupont, C. Rech, and R. Gules, "Reduced-order model and control approach for the boost converter with a voltage multiplier cell," *IEEE Trans. Power Electron.*, Vol. 28, No. 7, pp. 3395-3404, Jul. 2013.

[7] R. N. A. L. Silva, G .A. L. Henn, P. P. Praça, R. A. da Câmara, L. H. S. C. Barreto, and D. S. Oliveira Jr., "PID digital control applied to a high voltage gain converter with soft-switching cells," *Industrial Electronics (ISIE), 2010 IEEE International Symposium on.*, pp. 992–997, 2010.

[8] I. Laird and D. Dah-Chuan Lu, "High step-up DC/DC topology and MPPT algorithm for use with a thermoelectric generator," *IEEE Trans. Power Electron.*, Vol. 28, No. 7, pp. 740-741, Jul. 2013.

[9] D. H. Kim, S. Moon, C. I. Kim, and J.-H. Park, "Series-connected isolated-switched-capacitor boost converter," *IPEMC Power Electronics and Motion Control Conference*, Vol. 2, pp. 1343-1346, 2012.

[10] B. Gu, J. Dominic, J. S. Lai, Z. Zhao, and C. Liu, "High boost ratio hybrid transformer DC–DC converter for

photovoltaic module applications," *IEEE Trans. Power Electron*, Vol. 28, No. 4, pp. 2048 -2058, Apr. 2013.
[11] P. K. Peter and V. Agarwel, "Analysis and design of a ground isolated switched capacitor DC-DC converter," *Industrial Electronics (ISIE), 2010 IEEE International Symposium on*, pp. 632-637, 2010.
[12] S. Lee, P. Kim, and S. Choi, "High step-up soft-switched converters using voltage multiplier cells," *IEEE Trans. Power Electron*, Vol. 28, No. 7, pp. 3379-3387, Jul. 2013.
[13] M. Prudente, L. L. Pfitscher, G. Emmendoerfer, E. F. Romaneli, and R. Gules, "Voltage multiplier cells applied to non-isolated DC–DC converters," *IEEE Trans. Power Electron*, Vol. 23, No. 2, pp. 871-887, Mar. 2008.
[14] K. C. Tseng, C. C. Huang, and W. Y. Shih, "A high step-up converter with a voltage multiplier module for a photovoltaic system," *IEEE Trans. Power Electron*, Vol. 28, No. 6, pp. 3047-3057, Jun. 2013.
[15] D. Meneses, F. Blaabjerg, O. Garc´ıa, and J. A. Cobos "Review and comparison of step-up transformerless topologies for photovoltaic AC-module application," *IEEE Trans. Power Electron*, Vol. 28, No. 6, pp. 2649-2663, Jun. 2013.
[16] Q. Zhao and F. C. Lee, "High-efficiency, high step-up dc–dc converters," *IEEE Trans. Power Electron.,* Vol. 18, No. 1, pp. 65-73, Jan. 2003.
[17] K. C. Tseng and T. J. Liang, "Novel high-efficiency step-up converter," *Proc. Inst. Elect. Eng.-Elect. Power Appl*., Vol. 151, No. 2, pp. 182–190, Mar. 2004.
[18] T. J. Liang and K. C. Tseng, "Analysis of integrated boost-flyback step-up converter," *Proc. Inst. Elect. Eng.—Electr. Power Appl*., Vol. 152, No. 2, pp. 217–225, Mar. 2005.
[19] R. J. Wai and R. Y. Duan, "High step-up converter with coupled-inductor," *IEEE Trans. Power Electron.*, Vol. 20, No. 5, pp. 1025–1035, Sep. 2005.
[20] Y.-P. Hsieh, J.-F. Chen, and T.-J. Liang, "Novel high step-up DC-DC converter with coupled-inductor and switched-capacitor techniques for a sustainable energy system," *IEEE Trans. Power Electron.*, Vol. 26, No. 12, pp. 3481-3490, Dec. 2011.
[21] H. Cheng, K. M. Smedley, and A. Abramovitz, "Wide input wide output (WIWO) DC-DC converter," *IEEE Trans. Power Electron*., Vol. 25, No. 2, pp. 280-289, Feb. 2010.
[22] H. W. Seong, H. S. Kim, and K. B. Park, "High step-up DC-DC converters using zero-voltage switching boost integration technique and light-load frequency modulation control," *IEEE Trans. Power Electron.*, Vol. 27, No. 3, pp. 1383-1400, Mar. 2012.
[23] J. W. Ahn and D. H. Lee, "Performance of passive boost switched reluctance converter for single-phase switched reluctance motor," *Journal of Electrical Engineering & Technology,* Vol. 6, No. 4, pp. 505-512, Jul. 2011.
[24] Q. N. Trinh and H. H. Lee, "A new z-source inverter topology with high voltage boost ability," *Journal of Electrical Engineering & Technology*, Vol. 7, No. 5, pp. 714-723, Sep. 2012.
[25] Do-Hyun Kim and Joung-Hu Park, "High efficiency step-down flyback converter using coaxial cable coupled-inductor," *Journal of Power Electronics*, Vol. 13, No. 2, pp. 214-222, Mar. 2013.

**Do-Hyun Kim** received his B.S. degree from the Department of Electrical Engineering of Soongsil University, Seoul, Korea, in 2011. He is currently pursuing his M.S. degree at Soongsil University. His current research interests include the analysis and design of high-frequency switching converters and renewable energy applications.

**Jong-Ho Jang** received his B.S. degree from the Department of Electrical Engineering of Soongsil University, Seoul, Korea, in 2012. He is currently pursuing his M.S. degree at Soongsil University. His current research interests include the analysis and design of high-frequency switching converters and renewable energy applications.

**Joung-Hu Park** received his B.S., M.S., and Ph.D. degrees from the Department of Electrical Engineering and Computer Science of Seoul National University, Seoul, Korea, in 1999, 2001, and 2006, respectively. He is currently an assistant professor at Soongsil University, Seoul, Korea. His current research interests include the analysis of high-frequency switching converters and renewable energy applications.

**Jung-Won Kim** received his B.S., M.S., and Ph.D. degrees in electrical engineering from Seoul National University, Seoul, Korea, in 1994, 1996, and 2001, respectively. He became a senior engineer with Fairchild Korea Semiconductor, Ltd. He is currently a vice president of Silicon Mitus, Inc. His research interests include power factor corrections, converter parallel operation, modular converter system, distributed power systems, and soft switching converters.